

Switching between oscillations and homeostasis in competing negative and positive feedback motifs

Weihan Li^{a,b}, Sandeep Krishna^c, Simone Pigolotti^d, Namiko Mitarai^a, Mogens H. Jensen^{a,*}

^a*Niels Bohr Institute, University of Copenhagen, Blegdamsvej 17, 2100-DK, Copenhagen, Denmark.*

^b*Department of Biochemistry and Biophysics, University of California San Francisco, San Francisco, CA 94158, USA.*

^c*National Centre for Biological Sciences, Bangalore, Karnataka, India.*

^d*Dept. de Física i Eng. Nuclear, Universitat Politècnica de Catalunya Edif. GAIA, Rambla Sant Nebridi s/n, E-08222 Terrassa, Barcelona, Spain.*

Abstract

We analyze a class of network motifs in which a short, two-node positive feedback motif is inserted in a three-node negative feedback loop. We demonstrate that such networks can undergo a bifurcation to a state where a stable fixed point and a stable limit cycle coexist. At the bifurcation point the period of the oscillations diverges. Further, intrinsic noise can make the system switch between oscillatory state and the stationary state spontaneously. We find that this switching also occurs in previous models of circadian clocks that use this combination of positive and negative feedback. Our results suggest that real-life circadian systems may need specific regulation to prevent or minimize such switching events.

Keywords: negative feedback, positive feedback, oscillation, noise, circadian rhythm

1. Introduction

Genetic regulatory networks exhibit a wide range of oscillatory phenomena, ranging from the fast oscillations in calcium [1] to the 24 hour cycle of circadian clocks [2, 3]. The occurrence of oscillations is generally caused by the presence of a negative feedback loop in the regulatory network [4, 5]. From a theoretical point of view, negative feedback can cause a Hopf bifurcation and thus generate a transition between a stable fixed point, corresponding to homeostasis, and an attracting limit cycle, corresponding to oscillations.

*Corresponding author.

Email address: mhjensen@nbi.dk (Mogens H. Jensen)

However, in real regulatory networks, the loop causing oscillations is usually embedded in a larger network including multiple positive and negative feedbacks. In some cases, these additional loops have a demonstrable biological function, for example in giving tunability to the oscillation period [6] or in stabilizing the period of circadian clocks in the presence of temperature fluctuations or molecular noise [7]. In general, one expects that multiple feedback loops could lead to non-trivial behaviors from the viewpoint of bifurcation theory. The dynamics could become even richer when the noise induced by stochastic gene expression is taken into account. As we discuss later, circadian clocks are typical examples of genetic circuits where it may be important to understanding these effects.

In this paper, we present and analyze a class of network motifs in which a two-node positive feedback motif is inserted into a three-node negative feedback loop, as represented in Fig. 1. In section 2.1, we show that a deterministic dynamical models of the simplest of such networks, in a suitable parameter range, exhibits co-existence of a stable fixed point and a stable limit cycle. We explain this behavior in terms of a saddle-node separatrix-loop bifurcation [8], and show that it results in a diverging oscillation period close to the bifurcation point. In section 2.2, we use stochastic simulations using the Gillespie algorithm [9] to demonstrate that the noise can make the system switch between oscillatory state and the stationary state. We show that similar behaviour occurs in more realistic models of circadian clocks that contain the same combination of positive and negative feedback loops. Section 3 summarizes our thoughts on the relevance of these results for the behaviour of circadian clocks.

2. Results

2.1. Dynamics of the Network Motif

We study the class of genetic networks represented in Fig. 1. In each of the four networks, a positive feedback between node 1 and node 2 can give rise to a bi-stable switch. When node 3 is introduced, node 1, 2, 3 together form a negative feedback loop. The negative feedback loop tends to destabilize one of the stable fixed points of the switch. The simplest motifs that exhibit such “frustrated bistability” are studied in ref. [10]. Here, we study slightly larger networks which allow for more intricate dynamics, in particular a scenario where a stable limit cycle emerges around the unstable fixed point while the other stable fixed point remains unchanged.

We shall first focus our discussion on the network (a) in Fig 1, for which we write the following dynamical equations:

$$\frac{dx_1}{dt} = c + \frac{\alpha}{1 + (\frac{x_3}{k})^h} \frac{1}{1 + (\frac{x_2}{\beta k})^h} - \gamma x_1, \quad (1)$$

$$\frac{dx_2}{dt} = c + \frac{\alpha}{1 + (\frac{x_1}{k})^h} - \gamma x_2, \quad (2)$$

$$\frac{dx_3}{dt} = c + \frac{\alpha}{1 + (\frac{x_2}{k})^h} - \gamma x_3, \quad (3)$$

Here, $x_{1,2,3}$ are the concentrations of the proteins associated with the three nodes, α is the strength of the three inhibitory regulations, h is the Hill coefficient, c is a constant source term for each node, and γ is the degradation rate for each protein (we assume that all three proteins are stable, and therefore their degradation rate is determined by the cell division time). β is the control parameter to adjust the inhibition from node 2 to node 1. To simplify the equations, we introduce dimensionless parameters and variables $X_{1,2,3} = \frac{x_{1,2,3}}{k}$, $\tau = \gamma t$, $A = \frac{\alpha}{k\gamma}$, $B = \frac{c}{k\gamma}$:

$$\frac{dX_1}{d\tau} = B + A \frac{1}{1 + X_3^h} \frac{1}{1 + (\frac{X_2}{\beta})^h} - X_1 \quad (4)$$

$$\frac{dX_2}{d\tau} = B + A \frac{1}{1 + X_1^h} - X_2 \quad (5)$$

$$\frac{dX_3}{d\tau} = B + A \frac{1}{1 + X_2^h} - X_3. \quad (6)$$

We study this system of equations for parameter values of $h = 3, B = 0.1, A = 5$, and vary β as a control parameter, which changes the strength of the positive feedback relative to the negative feedback. We found three bifurcation points, at $\beta = \lambda_3 \approx 2.03$, $\beta = \lambda_2 \approx 1.923$, and $\beta = \lambda_1 \approx 1.45$. When $\beta > \lambda_3$ (Fig.2A), only one unstable fixed point and one stable limit cycle are found in the phase space. Here, the stable limit cycle is a global attractor. At $\beta = \lambda_3$, a saddle-node bifurcation occurs, where a stable fixed point and a saddle node emerge.

When $\lambda_2 < \beta < \lambda_3$ (Fig.2B), we find one stable limit cycle and three fixed points – one stable and two unstable. Within this region, the stable limit cycle is not the global attractor. Depending on the initial condition, the system may either reach the limit cycle or the stable fixed point. In the parameter range we studied, the volumes of the two basins of attraction are both non-negligible, separated by the surface shown in Fig 3.

Approaching the critical point λ_2 , the stable limit cycle approaches the saddle point, and eventually at $\beta = \lambda_2$ (Fig.2C), they generate a homoclinic cycle. When β is near λ_2 , the period of oscillation increases dramatically, and eventually diverges at the critical point $\beta = \lambda_2$ (Fig 4) as typical for homoclinic cycles. Such a bifurcation is classified as saddle-node separatrix-loop bifurcations [8, 11] and is a robust bifurcation scenario in a phase space of dimension

3 or more [8]. It corresponds to an attractor crisis, so that when β is reduced further, the stable limit cycle disappears. When $\lambda_1 < \beta < \lambda_2$ (Fig.2D), three fixed points still exist in the phase space: a stable fixed point, a saddle node and an unstable fixed point with complex eigenvalues. The stable fixed point is the global attractor. At $\beta = \lambda_1$, the saddle node and the unstable fixed point collide and disappear after a saddle-node bifurcation. So, when $\beta < \lambda_1$ (Fig.2E), there is only one fixed point, which is stable and is a global attractor.

The location and nature of the fixed points can be better understood by a graphical study of the intersections of the nullclines. We set $d/d\tau$ terms in equations (4)-(6) to zero, and rearrange the resulting algebraic relations to express X_2 and X_3 in terms of X_1 . Then, using this to eliminate X_2 and X_3 in equation (4) yields:

$$0 = \frac{A}{1 + \left(\frac{A}{1+X_1^h} + B\right)^h} \frac{1}{1 + \frac{A}{\beta(1+X_1^h) + \beta B}} + B - X_1. \quad (7)$$

Fig 2 right column shows the right hand side of Eq. (7) as the parameter β is varied. When $\beta > \lambda_3$ (Fig.2A), the function has one zero, corresponding to a unique unstable fixed point in phase space. When $\lambda_2 < \beta < \lambda_3$ (Fig.2B), $\beta = \lambda_2$ (Fig.2C) and $\lambda_1 < \beta < \lambda_2$ (Fig.2D), the function has two additional zeroes, indicating two more fixed points. From the eigen values of all three fixed points, one can show that only one of them (the circular one) is stable. Finally, when $\beta < \lambda_1$ (Fig.2E), the function has one zero again. Two fixed points disappear and only one stable fixed point remains.

We checked numerically the parameter range where the same bifurcations and qualitatively the same phase space portrait can be obtained. For $A = 5$ and $B = 0.1$, $h \gtrsim 3$ is required to see the same behavior. For $h = 3$ and $B = 0.1$, $A \gtrsim 3.5$ is required. The behavior is found to be insensitive to the value of B ; for $h = 3$ and $A = 5$, the behavior was unchanged for $0 \leq B \leq 100$. The same bifurcations can also be found in all the other 3 motifs listed in Fig 1. Namely, the observed sequence of bifurcations is a robust feature of such motifs.

2.2. Stochastic Dynamics

In this section, we investigate the effect of the intrinsic noise due to the discrete nature of molecular reactions in such motifs. We use the Gillespie algorithm [9] for stochastic simulations of the dynamical system specified by equations (1)–(3). We denote the copy number of molecules of species i as N_i .

The allowed transitions, along with their kinetic rates, are:

$$N_1 \xrightarrow{\frac{cV + \alpha V / [(1 + (N_3/k)^h)(1 + (N_2/\beta k)^h)]}{} N_1 + 1, \quad (8)$$

$$N_1 \xrightarrow{\gamma N_1} N_1 - 1, \quad (9)$$

$$N_2 \xrightarrow{\frac{cV + \alpha V / [(1 + (N_1/k)^h)]}{} N_2 + 1, \quad (10)$$

$$N_2 \xrightarrow{\gamma N_2} N_2 - 1, \quad (11)$$

$$N_3 \xrightarrow{\frac{cV + \alpha V / [(1 + (N_2/k)^h)]}{} N_3 + 1, \quad (12)$$

$$N_3 \xrightarrow{\gamma N_3} N_3 - 1. \quad (13)$$

To control the noise, we change the volume of the system V , which changes the production rates of N_i , but leaves the average concentration $x_i \equiv N_i/V$ constant, as long as the values of k, γ, h, c, α , and β are unchanged. The larger the value of V , and therefore the larger the copy numbers N_i , the smaller the noise (the relative fluctuations in N_i). Note that we do not explicitly consider processes like mRNA production, binding of transcription factors, etc. Inclusion of these steps can increase the noise in the system further [12].

Figure 5 shows the concentration N_i/V vs. time for a stochastic simulation in dimensionless units with $h = 3, B = 0.1, A = 5, \beta = 2$. We convert numbers so that the dimensionless concentration $X_i = 1$ corresponds to one molecule when volume $V = 1$, and simulated (A) $V = 1000$ and (B) $V = 100$. We can clearly see switching between the oscillatory state (the stable limit cycle) and the steady state (the stable fixed point), and this switching happens more often for smaller V , i.e., for larger noise.

To quantify this switching behavior, we measured the average switching time from the oscillatory state to the steady state and vice versa as a function of the system volume V (Fig.6). Because of the noisy dynamics, switching is determined by using two thresholds for the distance from the stable fixed point, S_1 and $S_2 > S_1$: We define a switching event from the steady regime to oscillatory regime when the distance exceeds S_2 , while the reverse switching happens when the distance becomes smaller than S_1 . Therefore, when the distance is between S_1 and S_2 , there is a history dependence in which regime the state belongs to. For this parameter set, the oscillation period is ~ 8.15 , thus we can see that the system with hundreds of molecules (corresponds to $V \approx 100$) can still cause frequent switching, on the order of once in every 10 oscillations. The switching rate decreases with V as expected. For large enough V , the switching rate decreases exponentially with V .

Finally, in order to see whether such switching behavior can be relevant for real biological systems, we study effect of noise on the more realistic model for *Drosophila* circadian rhythms described in ref. [13, 14]. The deterministic version of this model has a combination of several positive and negative feedback loops and exhibits the coexistence of a stable fixed point and a stable limit cycle [13]. We simulated the stochastic version of this model with parameters used in ref. [14]. A detailed description of the model and parameters are given in the

appendix. We observe again the switching between the oscillatory state and the steady state due to the noise (Fig 7). The switching is quite often compared to the oscillation frequency for the noise level expected for an average cell volume, i.e. $10^3 \mu m$ (Fig. 7C), where 1 [nM] corresponds to about 600 molecules¹.

3. Summary and Discussion

We have analyzed a class of network motifs consisting of a two-node positive feedback inserted into a three-node negative feedback loop. We demonstrated that a stable fixed point and a stable limit cycle can co-exist in this class of motifs. As parameters are changed, the system undergoes a saddle-node separatrix-loop bifurcation, with a diverging oscillation period as the system approaches the bifurcation. The location and nature of the fixed points were investigated in detail by outlining the intersections of the nullclines of the three variables. We then studied the effect of intrinsic noise to the motif, in the parameter regime where a fixed point and stable limit cycle co-exist. We showed that stochastic switching between the two happens with a rate that decreases with decreasing the level of the noise. Actually, our results complement the study in [25], where similar motifs for biochemical systems are studied focusing on the how a negative feedback perturbs the switch by positive feedback loops.

We further showed that similar behaviour is observed in a more complex model of the *Drosophila* circadian clock. This switching behaviour was not reported in a study of the effect of noise in a simplified version of the detailed model [7]. The studies on the *Drosophila* model [13, 14, 7] focused instead on the singular behaviour of the real circadian clock, where a single pulse of light can cause long-term suppression of the circadian rhythm [2, 15, 13]. The models explain this as a switch from the limit cycle to the stable fixed point, caused by a short external perturbation (the pulse of light) to some parameter values. Recent research suggests an alternate possibility, where the singular behaviour is caused by desynchronization of the clocks rather than stopping individual oscillations [16].

Our analysis of simple motif combining positive and negative feedback demonstrates that intrinsic noise, and not just external perturbations, can also cause switching where a limit cycle and a stable fixed point coexist in the phase space. As such repeated switching would disrupt the circadian rhythm, we can predict that specific regulatory mechanism must exist in real circadian clocks to suppress it. It would be interesting to explore the space of small network motifs to understand what mechanisms could implement this kind of suppression most effectively.

¹ Calculated based on $1 \text{ nM} \sim 6 \times 10^{23} \times 10^{-9}$ molecules per liter.

Acknowledgement

We thank Hiroshi Kori and Lei-han Tang for useful comments. This work is supported by the Danish National Research Foundation.

Appendix: The model for *Drosophila* circadian rhythm

We studied the stochastic version of the model for *Drosophila* circadian rhythm given in ref [14, 17]. The summary of the reactions in the model with deterministic equations of the model are shown in Fig. 8 with parameters given in the caption. We converted these equations into stochastic form using the Gillespie algorithm [9], as has been done to convert the simple motifs eqs. (1)-(3) to the stochastic version (8)-(13). The concentrations are converted to the number of molecules based on the typical cell volume of *drosophila*, about $1000\mu\text{m}^3$, which means 1 nM corresponds to about 600 molecules. Figure 7C is based on this conversion. For the case where the cell volume is 10 (100) fold bigger, the copy number is also converted to be 10 (100) fold bigger, which corresponds to the simulations shown in Fig. 7B (A).

References

- [1] S. Schuster, M. Marhl, and T. Hofer, Modelling of simple and complex calcium oscillations, *Eur. J. Biochem.* **269**, 1333-1355 (2002)
- [2] A.T. Winfree, *The Geometry of Biological Time*. New York: Springer, (1980).
- [3] B. Pfeuty, Q. Thommen, and M. Lefranc, Robust entrainment of circadian oscillators requires specific phase response curves, *Biophysical Journal* **100**, 2557 (2011).
- [4] G. Tiana, S. Krishna, S. Pigolotti, M.H. Jensen, K. Sneppen, Oscillations and temporal signalling in cells, *Phys. Biol.* **4** (2007) 45719-3.
- [5] S. Pigolotti, S. Krishna, M.H. Jensen, Oscillation patterns in negative feedback loops, *Proc. Natl. Acad. Sci.* **104** (2007) 65336537.
- [6] T.Y.C. Tsai, Y.S. Choi, W. Ma, J.R. Pomerening, C. Tang, J.E. Ferrell Jr., Robust, Tunable Biological Oscillations from Interlinked Positive and Negative Feedback Loops, *Science* **321** (2008), 126129.
- [7] D. Gonze, J. Halloy, A. Goldbeter, Robustness of circadian rhythms with respect to molecular noise, *Proc. Natl. Acad. Sci.* **99**(2002) 673-678.
- [8] N.A. Magnitskii, S.V. Sidorov, *New Methods for Chaotic Dynamics*, World Scientific Publishing Company, 2006.
- [9] D. T. Gillespie, Exact Stochastic Simulation of Coupled Chemical Reactions, *J. Phys. Chem.* **81** (1977) 2340-2361.
- [10] S. Krishna, S. Semsey and M. H. Jensen, Frustrated bistability as a means to engineer oscillations in biological systems *Phys. Biol.* **6** (2009) 036009.
- [11] E.M. Izhikevich, Neural Excitability, Spiking, and Bursting, *International Journal of Bifurcation and Chaos.* **10** (2000) 1171-1266.
- [12] A. Loinger, O. Biham, Stochastic simulations of the repressilator circuit, *Phys. Rev. E* **76**051917 (2007).
- [13] J.C. Leloup, A. Goldbeter, A molecular explanation for the long-term suppression of circadian rhythms by a single light pulse, *Am J Physiol Regulatory Integrative Comp Physiol.* **280** (2001) R1206R1212.
- [14] J.C. Leloup, D. Gonze, A. Goldbeter, Limit Cycle Models for Circadian Rhythms Based on Transcriptional Regulation in *Drosophila* and *Neurospora*, *J Biol Rhythms.* **14** (1999) 433-448.
- [15] S. Honma, K.I. Honma, Light-induced uncoupling of multioscillatory circadian system in a diurnal rodent, Asian chipmunk, *Am J Physiol Regulatory Integrative Comp Physiol.* **276** (1999) 1390-1396.

- [16] H. Ukai, T.J. Kobayashi, M. Nagano, K.H. Masumoto, M. Sujino, T. Kondo, K. Yagita, Y. Shigeyoshi, H.R. Ueda, Melanopsin-dependent photo-perturbation reveals desynchronization underlying the singularity of mammalian circadian clocks, *Nat Cell Biol* 9(2007), 1327-1334.
- [17] J.C. Leloup, A. Goldbeter, A Model for Circadian Rhythms in *Drosophila* Incorporating the Formation of a Complex between the PER and TIM Proteins, *J Biol Rhythms*. 13(1998) 70-87.
- [18] U. Schibler, P. Sassone-Corsi, A Web of Circadian Pacemakers, *Cell* 111 (2002), 919922.
- [19] L.P. Shearman, S. Sriram, D.R. Weaver, E.S. Maywood, I. Chaves, B. Zheng, K. Kume, C.C. Lee, T.J. van der Horst, M.H. Hastings, S.M. Reppert, Interacting Molecular Loops in the Mammalian Circadian Clock, *Science* 288 (2000), 1013-1019.
- [20] U. Albrecht, Invited Review: Regulation of mammalian circadian clock genes, *J Appl Physiol* 92 (2002), 13481355.
- [21] S.J. Aton, E.D. Herzog, Come Together, Right... Now: Synchronization of Rhythms in a Mammalian Circadian Clock, *Neuron*. 48 (2005), 531534.
- [22] U. Albrecht, G. Eichele, The mammalian circadian clock, *Curr Opin Genetics Dev* 13 (2003), 271277.
- [23] U. Albrecht, The mammalian circadian clock: a network of gene expression, *Frontiers in Bioscience* 9 (2004), 48-55.
- [24] F. Gachon, E. Nagoshi, S.A. Brown, J. Ripperger, U. Schibler, The mammalian circadian timing system: from gene expression to physiology, *Chromosoma* 113 (2004), 103112.
- [25] B. Pfeuty and K. Kaneko, The combination of positive and negative feedback loops confers exquisite flexibility to biochemical switches, *Phys. Biol.* 6 (2009), 046013.

Figure Captions

Figure 1: Four patterns of motifs, each consisting a switch and a negative feedback loop. Node 1 and node 2 form a switch. Node 1,2,3 form a negative feedback loop.

Figure 2: The left column is the real 3 dimensional phase space. The middle column is 2 dimensional illustration of the real phase space. The right most column shows the right hand side of Eq. (7). Parameters are set to be $h = 3$, $B = 0.1$, and $A = 5$. (A) $\lambda_3 < \beta$, with one stable limit cycle (line) and one unstable fixed point. (plot with $\beta = 2.2$) (B) $\lambda_2 < \beta < \lambda_3$, with three fixed points (an unstable fixed point with complex eigenvalue (square), saddle node (triangle) and a stable fixed point (circle)) and a stable limit cycle. (plot with $\beta = 2$) (C) $\beta = \lambda_2$, the saddle node hits the limit cycle and forms a homoclinic orbit. (plot with $\beta = 1.923$) (D) $\lambda_1 < \beta < \lambda_2$, there are only three fixed points. (plot with $\beta = 1.2$) (E) $\beta < \lambda_1$, there is only one stable fixed point. (plot with $\beta = 2$)

Figure 3: The stable limit cycle and the stable fixed point are shown by solid line and filled circle, respectively, for $h = 3$, $B = 0.1$, $A = 5$, and $\beta = 2$. The surface shows the boundary between the basin of attraction of the stable limit cycle and the basin of attraction of the stable fixed point.

Figure 4: Period of oscillations as a function of β , with $h = 3, B = 0.1, A = 5$. The period diverges at $\beta = \lambda_2 \approx 1.923$ (indicated by a vertical line), where a homoclinic cycle is present. As $\beta \rightarrow \infty$ the repressor link from node 2 to node 1 vanishes. What is left is a standard repressilator and the period one obtains in that limit (equal to 3.7 for these parameter values, shown by a horizontal line) is the period of this repressilator.

Figure 5: Time evolution of the concentrations for the stochastic simulation of the system with $h = 3, B = 0.1, A = 5, \beta = 2$. All the units are dimensionless, and concentrations are converted to the numbers so that $X_i = 1$ corresponds to one molecule when $V = 1$. (A) $V = 1000$ and (B) $V = 100$.

Figure 6: Switching rates from the oscillatory state to the steady state (open circles) and from the steady state to the oscillatory state (filled circles), as a function of system volume V , for the same parameter values as in Fig. 5. The threshold values are set to be $S_1 = 0.316, S_2 = 3.317$.

Figure 7: Intrinsic noise is introduced to the original model of Drosophila [13, 14]. Similar phenomena are observed. When cell size is very large, namely about 100 times of a typical cell volume, i.e. $10^5 \mu m$ (A), the system would switch from oscillation state to steady state at a random moment due to noise. As the cell size goes down ($10^4 \mu m$ in B, $10^3 \mu m$ in C), the switching becomes more and more frequent. A typical cell volumes for Drosophila is about $10^3 \mu m$ (C), which exhibit very noisy dynamics. Detailed description of the model with the parameter set is given in appendix, Fig. 8.

Figure 8: The model for Drosophila circadian rhythm given in ref [14, 17]. Negative feedbacks are shown with dotted line, while positive feedback loops are shown with dashed line. The deterministic equation of the model is shown in the right panel, where variables are concentrations of *per* (M_p) and *tim* (M_T) mRNAs, the PER and TIM with three phosphorylation levels of P_0 (T_0), P_1 (T_1), and P_2 (T_2), respectively, the PER-TIM complex C , and the nuclear form of the PER-TIM complex (C_N). Parameters used are: $n = 4, v_{sP} = 1.1$ nM/h, $v_{sT} = 1$ nM/h, $v_{mP} = 1.0$ nM/h, $v_{mT} = 0.7$ nM/h, $v_{dP} = 2.2$ nM/h, $k_{sP} = k_{sT} = 0.9$ /h, $k_1 = 0.8$ /h, $k_2 = 0.2$ /h, $k_3 = 1.2$ /(nM·h), $k_4 = 0.6$ /h, $K_{mP} = K_{mT} = 0.2$ nM, $K_{IP} = K_{IT} = 1$ nM, $K_{dP} = K_{dT} = 0.2$ nM, $K_{1P} = K_{1T} = K_{2P} = K_{2T} = K_{3P} = K_{3T} = K_{4P} = K_{4T} = 2$ nM, $V_{1P} = V_{1T} = 8$ nM/h, $V_{2P} = V_{2T} = 1$ nM/h, $V_{3P} = V_{3T} = 8$ nM/h, $V_{4P} = V_{4T} = 1$ nM/h, $k_d = k_{dC} = k_{dN} = 0.01$ /h, $V_{dT} = 1.3$ nM/h.

Figure 1

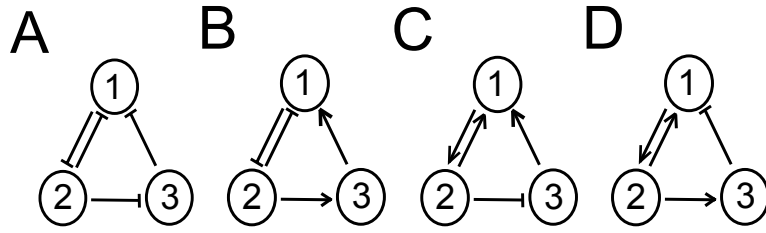


Figure 2

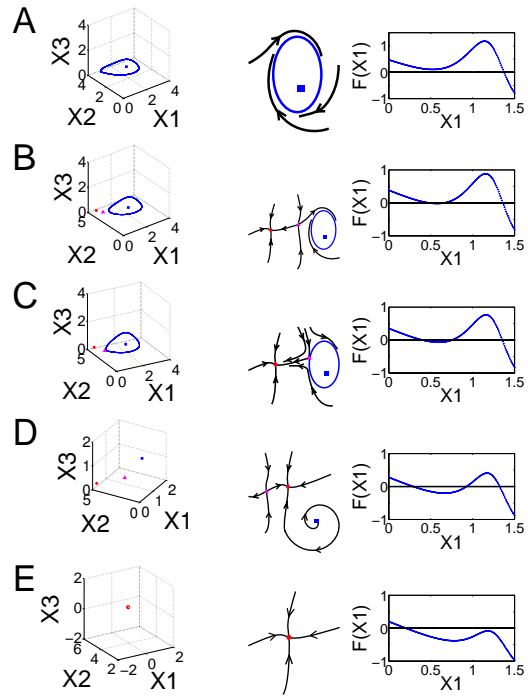


Figure 3

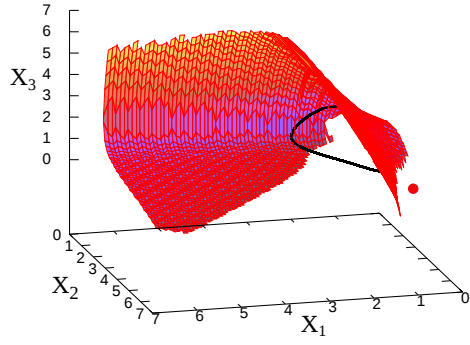


Figure 4

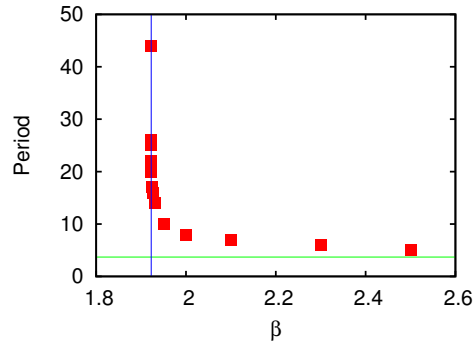


Figure 5

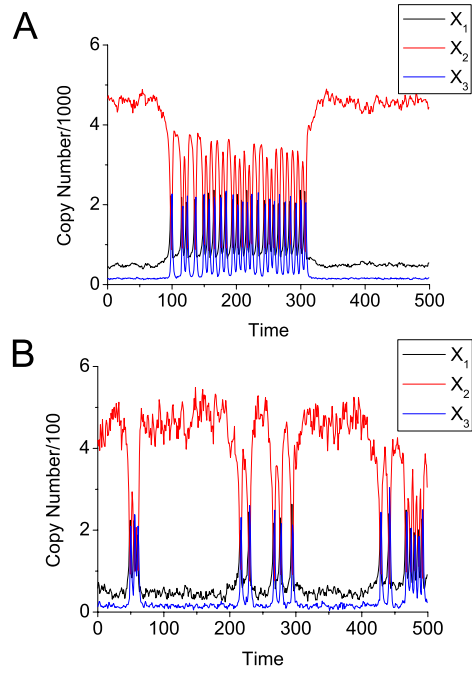


Figure 6

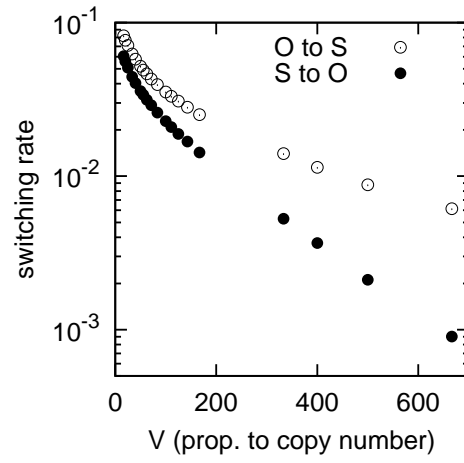


Figure 7

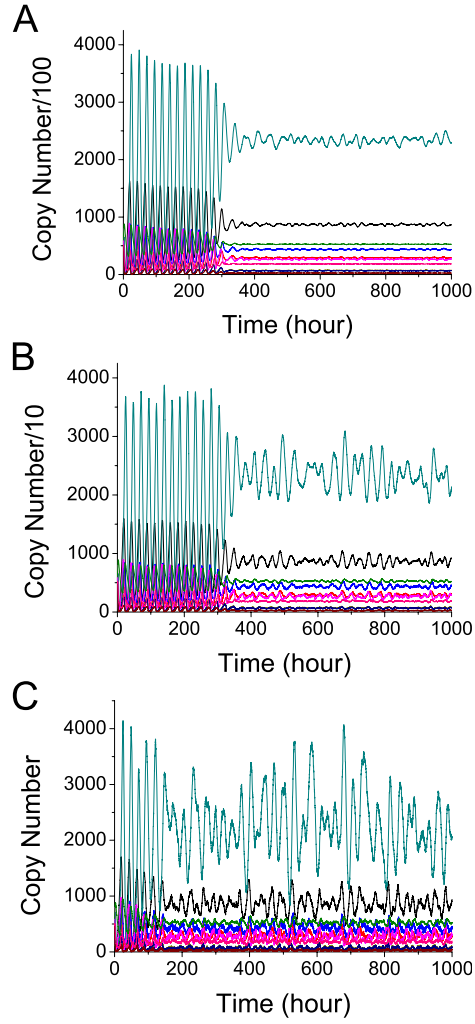


Figure 8

